



LCC-0106  
CBN 02-10  
October 2002

Linear Collider Collaboration Tech Notes

---

# Pulsed Helical Undulator for Test at SLAC Polarized Positron Production Scheme

Alexander A. Mikhailichenko

Cornell University  
LEPP  
Ithaca, New York

Abstract: We represent here parameters and some details of calculations done for a pulsed helical undulator with period 2 mm. This undulator is planned for experiment suggested for test at SLAC polarized positron production scheme.

# PULSED HELICAL UNDULATOR FOR TEST AT SLAC THE POLARIZED POSITRON PRODUCTION SCHEME. BASIC DESCRIPTION.

Alexander A. Mikhailichenko  
*Cornell University, LEPP, Ithaca, NY 14853*

We represent here parameters and some details of calculations done for pulsed helical undulator with period 2mm. This undulator is planned for experiment suggested for test at SLAC polarized positron production scheme.

## INTRODUCTION

We continuing here description of components of the scheme for polarized positron production [1] supposed to be tested at SLAC.

One meter long pulsed undulator having 6 mm period and the axis field  $\sim 6kG$  ( $K \cong 0.35^1$ ) was successfully tested many years ago [2, 3]. The feeding current in a wire with  $1 \times 1 \text{ mm}^2$  cross section was  $\sim 10 \text{ kA}$ . Pulse duration was  $\sim 50 \mu\text{sec}$ , feeding voltage  $\sim 1.19 \text{ kV}$  required by inductance  $\sim 1.3 \mu\text{H}$  allowed operation with repetition rate of  $25\text{Hz}^2$ . Such high current (and inductance) was forced by the aperture clearance of 4mm in diameter required.

The idea to test the method of polarized positron production at SLAC was materialized recently [4,5]. As the length of the testing device is one meter only rather than a hundred meters in full project, the aperture of the undulator can be shrunk to  $\sim 1\text{mm}$  clearance. The concept of pulsed helical undulator suitable for this test was described in [6], Fig.1. As the SLAC energy is going to be more likely  $\sim 47 \text{ GeV}$ , rather than  $50 \text{ GeV}$ , this forced to reduce period of undulator closer to 2mm. So we decided to refresh the parameter list as well as to add some details into description of the undulator together with necessary formulas.

Let us remind first, that the undulator has two helixes shifted in longitudinal direction by half of period. Technology for manufacturing of double helix with period 2.4 mm was tested successfully [6] and there was not found any limitation to make the windings with period 2 mm.

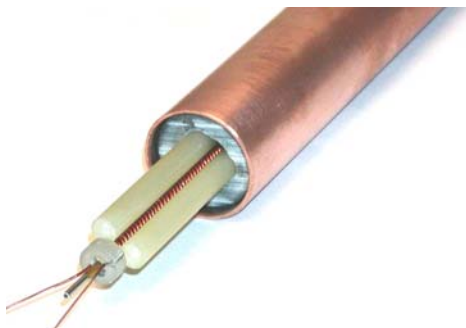


**FIGURE 1:** Model of pulsed undulator with period of 2.42 mm and 231.5 mm long [6]. Three G-10 rods squeezed with help of short rings having cylindrical grooves. This arrangement serves as a positioning system

<sup>1</sup> This value is optimal for 150 GeV primary beam.

<sup>2</sup> Required by VLEPP parameters at that time.

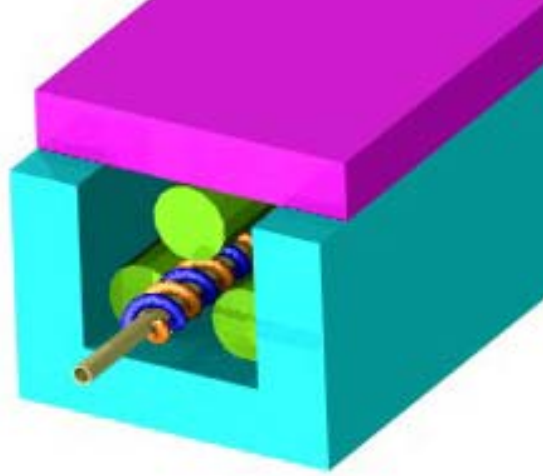


**FIGURE 2:** Another concept of fixture the rods. Two G10 rods are based in corners of long groove. Third rod with help of strip spring compresses the windings to the other two ones.

In Fig.2, the transverse position of the helixes is well established in a slightly different way. Upper rod might have grooves with period of helix, fixing longitudinal positions of the wires [2,6]. The StSt tube id diameter suggested for now to be 0.889mm, the OD diameter -1.0668 mm.

In this publication we will concentrate on the physical part of the project, however.

## FIELDS IN AN UNDULATOR

Fields in an undulator as in any magnet can be calculated analytically as well as numerically with help of appropriate 3D code. We used both ways for evaluation of the fields in undulator. Both gave the same results.

Lower we will suggest that the feeding current is steady as the time of the beam passage through the undulator is much less, than suggested duty time (30  $\mu s$ ). So the radiation was calculated.

For analytical calculation the easiest way is to use expressions derived in [7] for the vector potential of a pair of thin helical strips caring each opposite current values  $\pm I$ , wounded on cylindrical surface as (SI units)

$$A_\varphi + iA_\rho(\rho, \varphi, z) = \frac{\mu_0 I \cdot ctg\psi}{\pi} \left\{ \sum_m^{1,3,5,\dots} e^{im\left(\varphi - \varphi_0 - \frac{2\pi z}{\lambda_u}\right)} \frac{\sin(m\alpha)}{m\alpha} \times I_{m-1}\left(m\frac{2\pi\rho}{\lambda_u}\right) K_{m-1}\left(m\frac{2\pi a}{\lambda_u}\right) + \sum_m^{1,3,5,\dots} e^{-im\left(\varphi - \varphi_0 - \frac{2\pi z}{\lambda_u}\right)} \frac{\sin(m\alpha)}{m\alpha} \times I_{m+1}\left(m\frac{2\pi\rho}{\lambda_u}\right) K_{m+1}\left(m\frac{2\pi a}{\lambda_u}\right) \right\}, \quad (1)$$

$$A_z(\rho, \varphi, z) = \frac{2\mu_0 I}{\pi} \left\{ \sum_m^{1,3,5,\dots} \cos\left[m\left(\varphi - \varphi_0 - \frac{2\pi z}{\lambda_u}\right)\right] \times \frac{\sin(m\alpha)}{m\alpha} \times \left[ I_m\left(m\frac{2\pi\rho}{\lambda_u}\right) K_m\left(m\frac{2\pi a}{\lambda_u}\right) \right] \right\}, \quad a \geq \rho \geq 0,$$

where  $a$  is the radius of the cylinder,  $\lambda_u$  is period of winding,  $\varphi_0$  is the local angle between mid of the strip and axis  $x$ ,  $ctg\psi = 2\pi a / \lambda_u$  is a winding (pitch) angle of helix,  $2\alpha$  represents the angle under which the strip is visible from the central axis.

Transverse magnetic field can be calculated from these expressions using formula  $\vec{B} = \text{rot}\vec{A}$  written in cylindrical coordinates as the following

$$B_{\varphi}(\rho, \varphi, z) = \frac{2\mu_0 I}{\pi\rho} \text{ctg}\psi \left\{ \sum_m^{1,3,5,\dots} m \cdot \frac{\sin(m\alpha)}{m\alpha} \cos\left[m\left(\varphi - \varphi_0 - \frac{2\pi z}{\lambda_u}\right)\right] \times \left[ I_m\left(m\frac{2\pi\rho}{\lambda_u}\right) K'_m\left(m\frac{2\pi a}{\lambda_u}\right) \right] \right\}. \quad (2)$$

For the field on the diameter line connecting two wires centers of symmetry  $\varphi = \varphi_0 + 2\pi/\lambda_u$  and expression for the field comes to

$$B_{\varphi}\left(\rho, \varphi_0 + \frac{2\pi z}{\lambda_u}, z\right) = \frac{2\mu_0 I}{\pi\rho} \left(\frac{2\pi a}{\lambda_u}\right) \sum_m^{1,3,5,\dots} m \cdot \frac{\sin(m\alpha)}{m\alpha} \times I_m\left(m\frac{2\pi\rho}{\lambda_u}\right) K'_m\left(m\frac{2\pi a}{\lambda_u}\right), \quad a \geq \rho \geq 0. \quad (3)$$

what means that in rotating with period of winding coordinate system the field is constant at fixed radius.

For the field at the axis

$$\begin{aligned} H_{\varphi}(0,0,z) &= -\frac{I}{\pi a} \times \left(\frac{2\pi a}{\lambda_u}\right) \times \cos\left(\frac{2\pi z}{\lambda_u}\right) \times \left\{ \left(\frac{2\pi a}{\lambda_u}\right) K_0\left(\frac{2\pi a}{\lambda_u}\right) + K_1\left(\frac{2\pi a}{\lambda_u}\right) \right\} = \\ &= \frac{I}{\pi a} \times \left(\frac{2\pi a}{\lambda_u}\right)^2 \times \cos\left(\frac{2\pi z}{\lambda_u}\right) \times K'_1\left(\frac{2\pi a}{\lambda_u}\right). \end{aligned} \quad (4)$$

This formula illustrated in Fig.3.

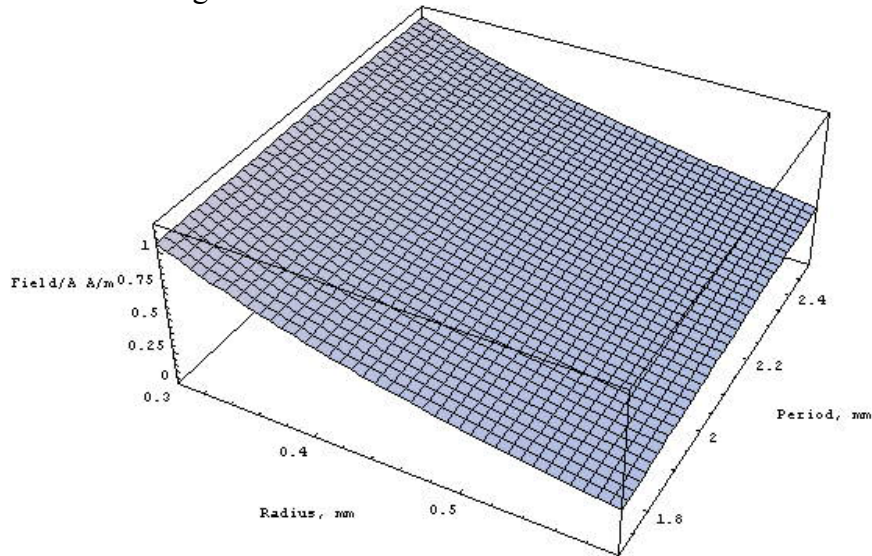


**FIGURE 3:** 3D plot based on formula (4). Current  $I=1A$ .

For the energy stored in magnetic field we have expression  $W = \frac{1}{2}LI^2 = \frac{1}{2} \int (\vec{i} \cdot \vec{A})dV$ , where  $L$  is inductance. Using formulas (1) it is possible to obtain inductance per unit length as the following, [7]

$$L_l(\lambda_u, a, \alpha) = -\frac{4\mu_0}{\pi} \cdot \left(\frac{2\pi a}{\lambda_u}\right)^2 \sum_m^{1,3,5,\dots} \left(\frac{\sin(m\alpha)}{m\alpha}\right)^2 \times I'_m\left(m \cdot \frac{2\pi a}{\lambda_u}\right) \cdot K'_m\left(m \cdot \frac{2\pi a}{\lambda_u}\right). \quad (5)$$

For the conductor of finite size and shape, the expression for the vector potential and fields can be represented as a sum of terms (1,2) with appropriately varying  $\alpha_i, a_i$  for each layer. The current in each layer  $I_i$  must be calculated also taking into account the shape of conductor. Naturally  $I = \sum_i I_i$ . Here, however there is some uncertainty associated with proper current

distribution. For helical geometry of the wire, the current has a tendency to run in the inner layer as the path here is shorter.

In our design we calculating the fields with round wire as well as rectangular one. On the basis of result obtained from here, we make final conclusion. The difference between these two cases in of the order of 12-15% however in a favor of rectangular wire.

The type of field representation described above was used in [3,8] for the field calculation in helical undulator and we are using it here for some extend below. Numerical calculations represented here done with 3D code MERMAID.

Let us represent also some simplifications of (2) what might be useful for analytical evaluations in future. Derivative of the Bessel function (of the second kind) can be expressed as the following

$$\begin{aligned} K'_m(x) &= -\frac{1}{2}[K_{m-1}(x) + K_{m+1}(x)] \\ -xK'_m(x) &= x \cdot K_{m-1}(x) + m \cdot K_m(x). \end{aligned} \quad (6)$$

With these formulas the expression for magnetic field (2) can be represented as the following

$$B_\varphi = -\frac{\mu_0 I}{\pi \rho} \cdot \left(\frac{2\pi a}{\lambda_u}\right) \cdot \left\{ \sum_m^{1,3,5,\dots} \frac{\sin(m\alpha)}{\alpha} \cos\left(m\left(\varphi - \varphi_0 - \frac{2\pi z}{\lambda_u}\right)\right) \times I_m\left(m \frac{2\pi \rho}{\lambda_u}\right) \left[ K_{m-1}\left(\frac{2\pi m a}{\lambda_u}\right) + K_{m+1}\left(\frac{2\pi m a}{\lambda_u}\right) \right] \right\} \quad (7)$$

Bessel functions in its turn can be expressed as the following, (see for example [9])

$$I_m(x) = i^{-m} J_m(ix) = \frac{x^m}{2^m m!} \left\{ 1 + \frac{x^2}{2(2m+2)} + \frac{x^4}{2 \cdot 4(2m+2)(2m+4)} + \dots \right\} = \sum_{k=0}^{\infty} \frac{(x/2)^{m+2k}}{k!(m+k)!},$$

$$I_{-m}(x) = I_m(x),$$

$$\begin{aligned} K_m(x) &= (-1)^{m+1} \{ \ln(x/2) + \gamma \} \cdot I_m(x) + \frac{1}{2} \sum_{k=0}^{\infty} (-1)^k (m-k-1)! \left(\frac{x}{2}\right)^{2k-m} + \\ &+ \frac{(-1)^m}{2} \sum_{k=0}^{\infty} \frac{(x/2)^{m+2k}}{k!(m+k)!} \{ \Phi(k) + \Phi(m+k) \}. \end{aligned} \quad (8)$$

Where  $\Phi(k) = 1 + \frac{1}{2} + \frac{1}{3} + \dots + \frac{1}{k}$ ,  $\Phi(0) = 0$ ,  $\gamma = 0.5772156\dots$  is Euler's constant.

For many cases the only first longitudinal harmonics is important. This defined by how much the particle is shifted from the central axis ( $\rho$  value) and by  $a/\lambda_u$  ratio. We will see (Fig.10) that even for  $\rho/a \approx 1$  description with 3 longitudinal harmonics is acceptable. So for the first harmonics

$$H_\varphi = -\frac{I}{\pi\rho} \cdot \left(\frac{2\pi a}{\lambda_u}\right) \cdot \frac{\sin(\alpha)}{\alpha} \cos\left(\varphi - \varphi_0 - \frac{2\pi z}{\lambda_u}\right) \times I_1\left(\frac{2\pi\rho}{\lambda_u}\right) \left[ K_0\left(\frac{2\pi a}{\lambda_u}\right) + K_2\left(\frac{2\pi a}{\lambda_u}\right) \right] \quad (9)$$

The terms in rectangular brackets are the constants depending on ratio of diameter to the period, which is about  $2\pi a/\lambda_u \equiv \pi(2a)/\lambda_u \equiv \pi/2$  in our case, so  $K_0(\pi/2) + K_2(\pi/2) \equiv 0.71$ . For a thin conductor also  $\sin\alpha/\alpha \equiv 1$ , so expanding  $I_1(x) = \frac{x}{2} + \frac{x^3}{2^2 \cdot 4} + \frac{x^5}{2^4 \cdot 4^2 \cdot 6} + \frac{x^7}{2^2 \cdot 4^2 \cdot 6^2 \cdot 8} + \dots$  one can obtain dependence of magnetic field on transverse coordinate,  $x = 2\pi\rho/\lambda_u \equiv \rho/\tilde{\lambda}_u$

$$\begin{aligned} H_\varphi &= -\frac{0.71}{2} \frac{I}{\tilde{\lambda}_u} \cdot \cos\left(\varphi - \varphi_0 - \frac{2\pi z}{\lambda_u}\right) \times I_1\left(\frac{2\pi\rho}{\lambda_u}\right) / \left(\frac{2\pi\rho}{\lambda_u}\right) \equiv \\ &\equiv -\frac{0.71}{4} \frac{I}{\tilde{\lambda}_u} \cdot \cos\left(\varphi - \varphi_0 - \frac{2\pi z}{\lambda_u}\right) \times \left[ 1 + \frac{1}{8} \left(\frac{\rho}{\tilde{\lambda}_u}\right)^2 + \frac{1}{768} \left(\frac{\rho}{\tilde{\lambda}_u}\right)^4 + \dots \right] \end{aligned} \quad (10)$$

Normally the terms in rectangular brackets describe the dipole, sextupole, decapole, ... fields responsible for the perturbation of emittance of a primary beam as a result of motion in nonlinear fields. What is important here is that the measure of these effects is the ratio of the beam size to the period of undulator  $(\rho/\tilde{\lambda}_u)^2/8 \equiv \varepsilon\beta/\tilde{\lambda}_u^2/8$ , where  $\varepsilon$  is emittance of the beam and  $\beta$  is envelope function. We will describe these effects in separate publications.

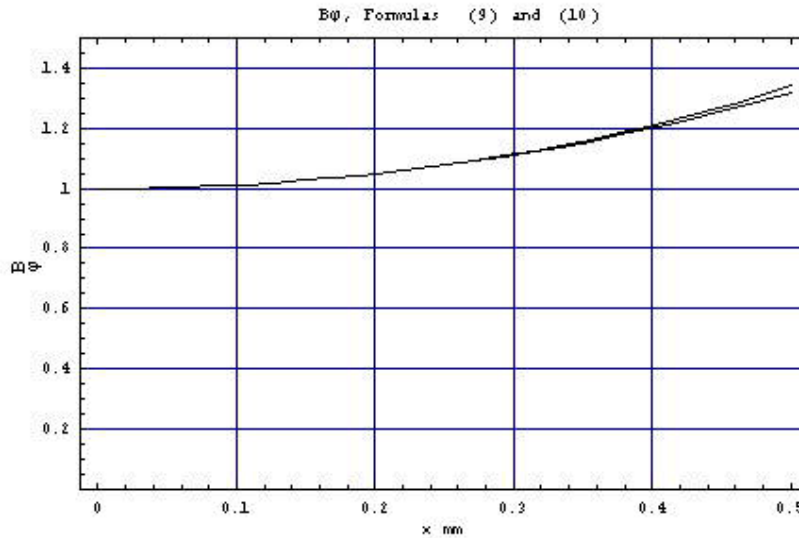
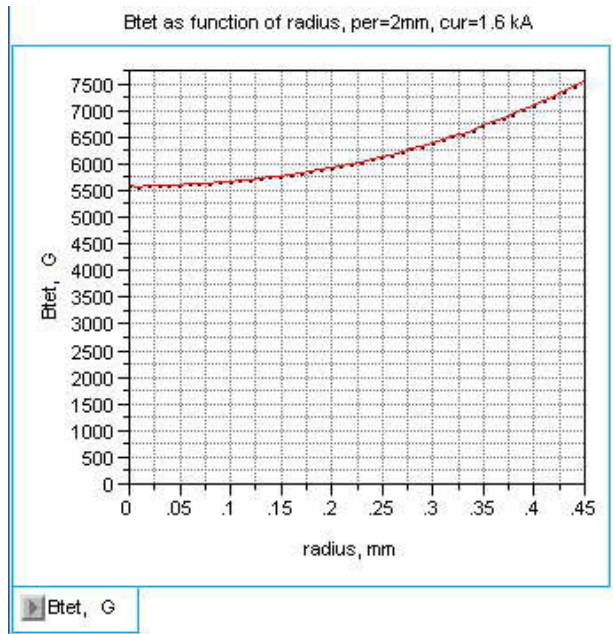


FIGURE 4: Exact solution (9) and approximation with three terms (10).

One can see, that the difference in magnetic field values obtained with formulas (9) and (10) at 0.45 mm is less than 2%,

For SLAC emittance  $\gamma\varepsilon \cong 3 \times 10^{-3}$  cm×rad in a crossover of envelope function having value there  $\beta_0 \cong 300$ cm sigma of the beam goes to  $\sigma \cong \sqrt{(\gamma\varepsilon)\beta_0/\gamma} \cong 3 \times 10^{-3}$ cm. At 0.3 mm, what is ten sigma, the field deviation from constant is ~10%. On the Figures 5-11 there are represented different field distributions obtained with formulas described above.



**FIGURE 5:** Transverse distribution of the field (Gauss) across the line connecting the centers of conductors.

Radius of the winding in all examples is  $a=0.5$ mm, period  $\lambda_u = 2$  mm, feeding current is 1.6kA. Factor undulatority  $K = eH\lambda_u / 2\pi mc^2 \cong 93.4 \cdot H(T) \cdot \lambda_u(m)$  for these parameters goes to  $K = 0.1$ . Heating per pulse with 30  $\mu$ sec duty time goes to  $\sim 3^\circ C$ /pulse. Voltage required to support the current 1.6kA goes to  $\sim 1.7$  V/cm.

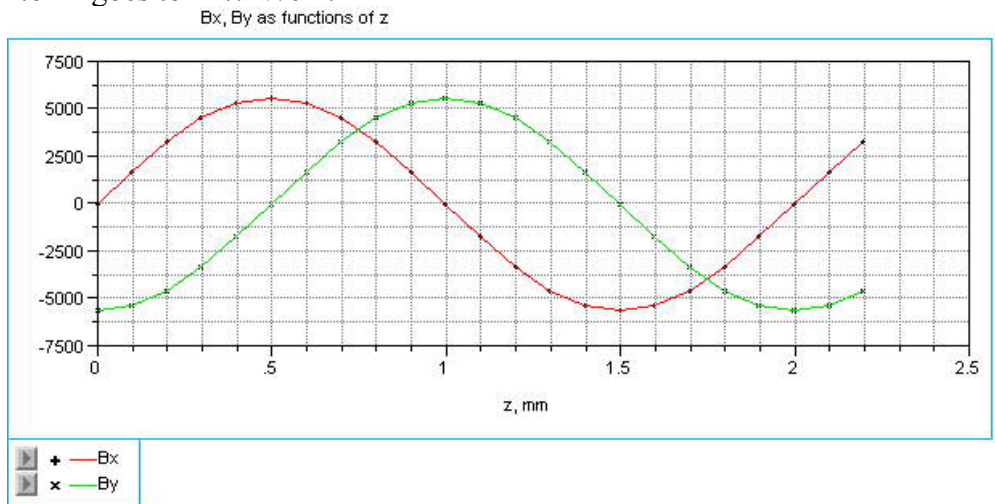


**FIGURE 6:** Transverse components of magnetic field, G on axis as functions of longitudinal coordinates. Longitudinal component of the field is absent. Period of undulator is 2 mm, feeding current 1.6kA. Lines are pure sin/cos ones.

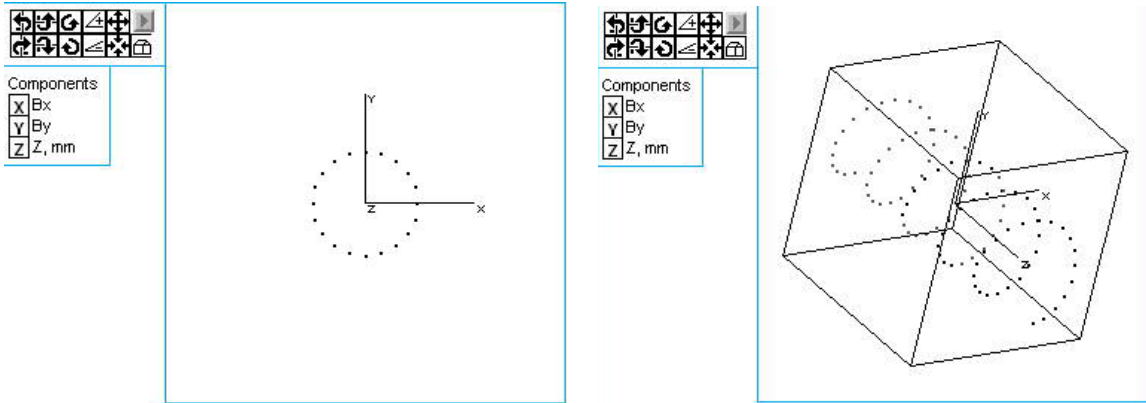


**FIGURE 7:** Vectorial visualization of the transverse fields at the axis of helical undulator from Fig.6. The dots are representing the ends of the vector of magnetic field components  $B_x$ ,  $B_y$  as a function of transverse coordinate. Center of the helix coincides with line  $\{x=0,y=0\}$ . At the left- the front view of the helix is represented.

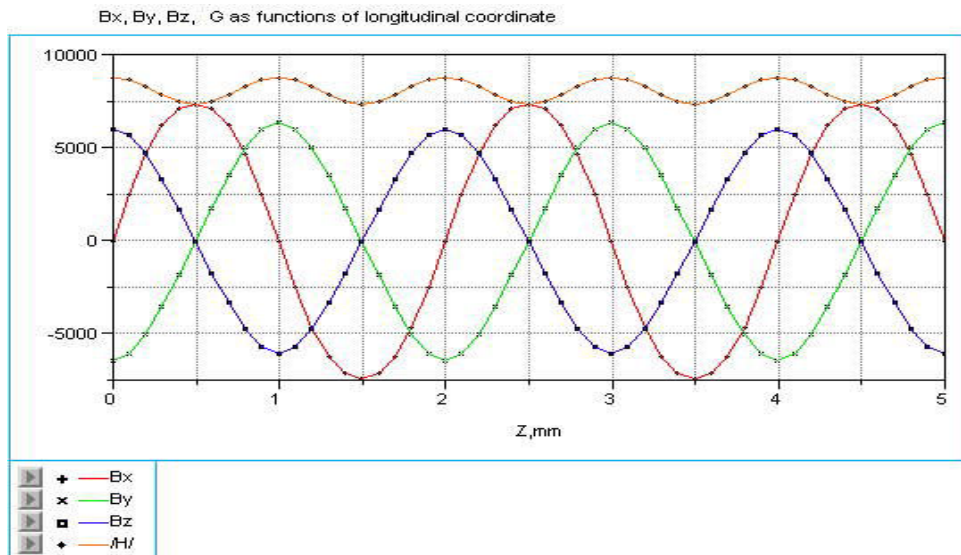


**FIGURE 8:** Longitudinal axis is now shifted in radial direction on  $\Delta r = 0.3$  mm. In such a way the fields look for ultrarelativistic particle moving along this line. Feeding current 1.6kA.

One can see, that in this case the curves remains sinusoidal. The longitudinal field rises to the significant value  $\sim 6$  kG.

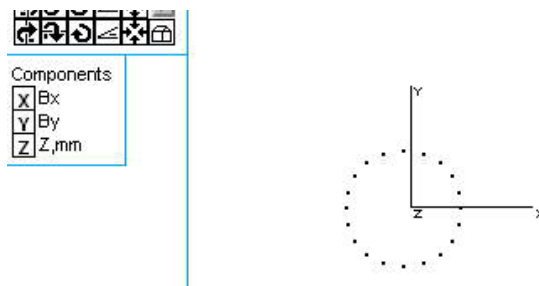


**FIGURE 9:** Vectorial visualization for the fields on shifted axes from Fig.4. One can see that in this case ends of magnetic field vector remain on just slightly deformed circle, but with shifted center. The shift is equal to the field value at  $\Delta r = 0.3$  mm. Ellipticity remains small.

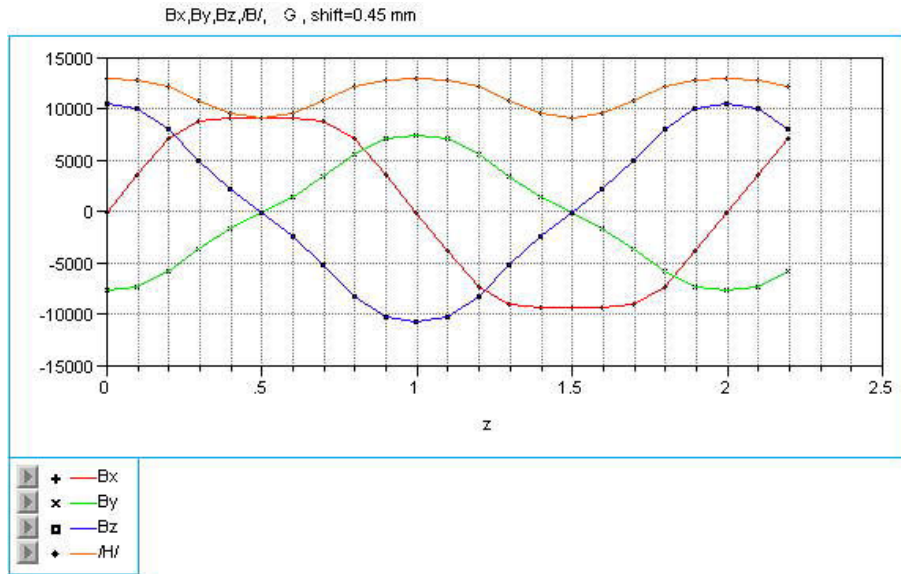


**FIGURE 10:** Longitudinal axis is now shifted in radial direction on  $\Delta r = 0.45$  mm, practically to the edge of the wire. One can see, that the field value module is about twice of that was at center. Feeding current 1.6 kA.

One can see from Fig.10, that the field becomes significantly non sinusoidal in longitudinal direction, requiring few longitudinal harmonics for description.

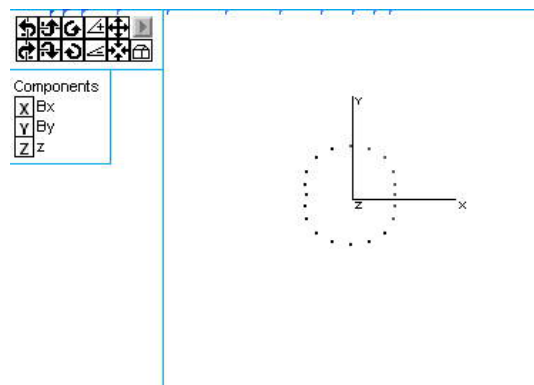


**FIGURE 11:** Vectorial visualization for the fields on shifted axes from Fig.6. One can see that in this case ends of magnetic field vector are deflected from circle. Average radius of this oval is about to be twice as on Figs. 7 and 9.

3D code MERMAID allowing calculation 3D field distribution as well as energy stored in magnetic field per longitudinal unit.

As we mentioned above the current distribution inside the wire need to be evaluated in additional run. In [13] there was made an estimation of the current distribution, however for infinitesimal in thickness winding. In this case the current distribution is the value of the magnetic field distribution divided by magnetic permeability of vacuum  $\mu_0$ .

In reality the current distribution in the wire need to be calculated as a solution of equation  $div \vec{j} = 0$  with appropriately given boundary condition. In MERMAID the current distribution obtained in a separate run. Boundary conditions are given as the points, where the currents enter the wires. Also there is some perturbations of the field due to the effect of establishing the equilibrium current distribution inside the wire, by choosing the entrance point for the current far

enough from the region of interest, one can diminish this effect. Typically the end fields are the mostly interesting ones. So choosing the geometry starting few periods from the ends is enough for proper modeling.

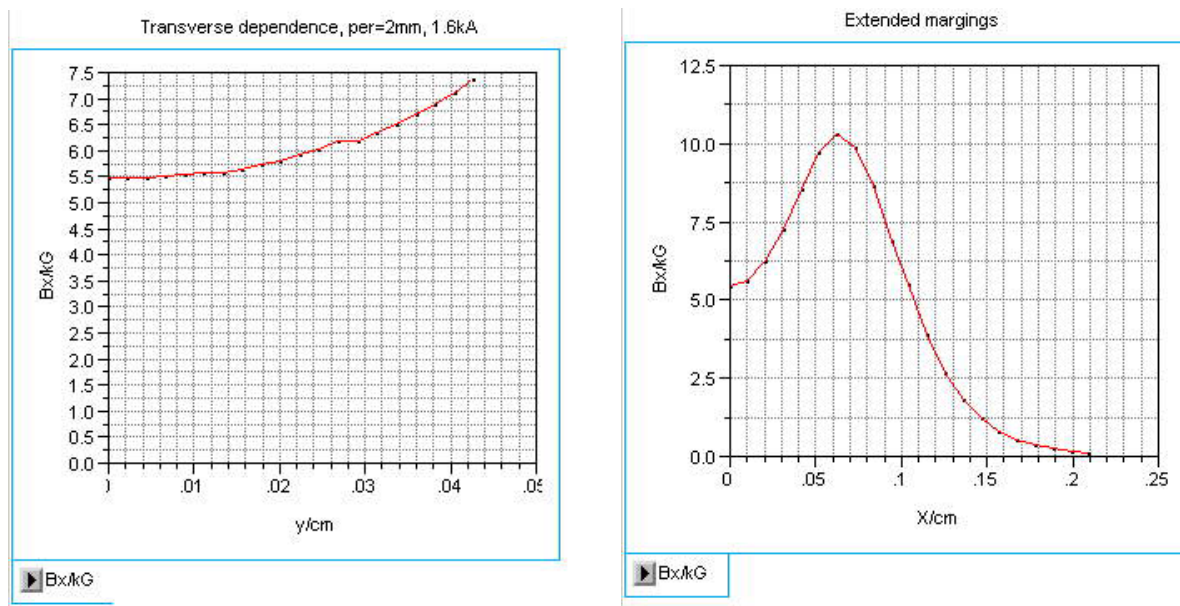


**FIGURE 12:** Field profile across undulator aperture starting from the center. Feeding current 1.6 kA. Calculations have done with MERMAID.

Left graph on Fig.12 must be compared with one in Fig.5, where the same transverse dependence, but calculated analytically is represented. One can see, that agreement is very good. At the right in Fig.12, the same transverse dependence with extended limits is represented. Wire occupies the distance from 0.05 to 0.1 cm in this picture. The slice line is going between the wires. One can see, that behind 2.1 mm from center, the field is practically absent. This gives an idea on how close the walls in Fig.2 can go to the helix. So the window in Fig.2  $1 \times 1 \text{ cm}^2$  is enough for the helix positioning avoiding influence of surroundings.

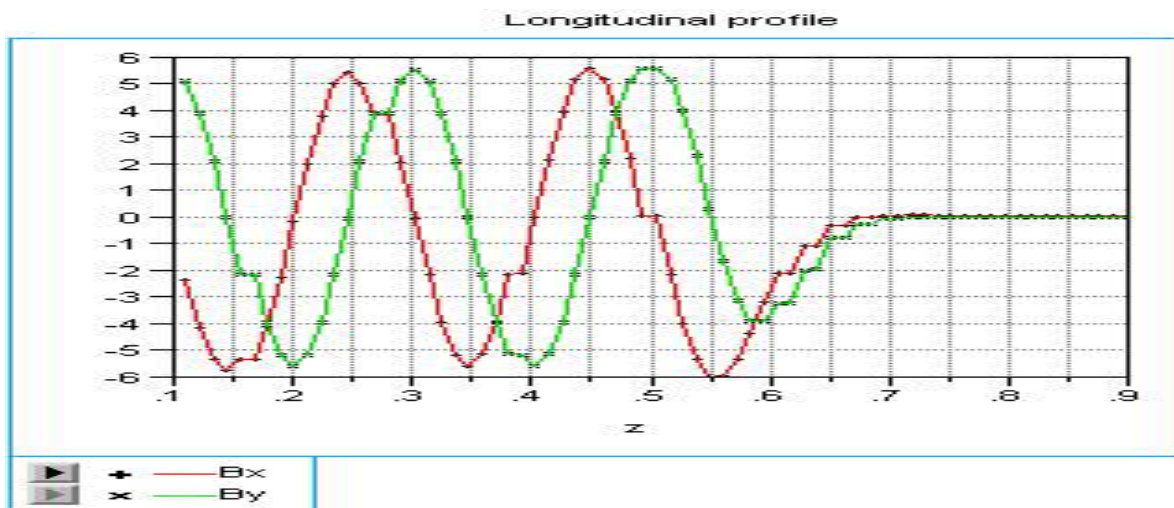


**FIGURE 13:** Longitudinal field profile, kG along undulator aperture around the end, cm. There is no end correction.

Longitudinal profile is represented in Fig.13. This type of field mapping used for modeling end field effects (will be described separately).

For testing of analytical formulas the measurements were done many years ago with scaled models of undulators. Winding radius was about 2 cm and wires were  $1 \times 1 \text{ cm}^2$ , period 42 mm. Hall probe was easily moved between wires. Transverse and longitudinal dependence of the field like the one represented in Figs.12 was measured and compared with calculated, showing good agreement [2].

## RADIATION

Radiation was investigated in many publications. Pioneering among them is [10]. As the fields in undulator can be treated as pure sinusoidal ones as functions of longitudinal coordinate, one can obtain the formulas for radiation rather easily after all. We will refer to [11] however. This publication contains all references (see also [12]<sup>3</sup>).

For the full intensity we have the expression

$$I_{tot} = \frac{2}{3} \frac{\Omega^2}{c} e^2 K^2 \gamma^2 = \frac{2}{3} mc^2 \cdot c \cdot r_o K^2 \gamma^2 / \lambda_u^2, \quad (11)$$

where  $r_o = e^2 / mc^2$  is a classical electron radius,  $\Omega = 2\pi c / \lambda_u \equiv c / \lambda_u$  is transverse oscillation frequency,  $\gamma = E / mc^2$ . So the rate of energy losses is given by

$$\frac{d\gamma}{cdt} \cong -\frac{2}{3} r_o \frac{K^2}{\lambda_u^2} \gamma^2. \quad (12)$$

One can see that intensity and  $d\gamma / cdt$  are not functions of the undulator period.

Radiation coming from helical undulator can be represented as a sum of harmonics, associated with period of the undulator which is basically the frequency of spontaneous radiation

$$\begin{aligned} \omega_n = n\omega_1 &= \frac{n\Omega}{1 - \beta \bar{e}} \cong \frac{n\Omega}{1 - \beta_{\parallel} \cos \vartheta} \cong \frac{n\Omega}{1 - \beta_{\parallel} \cdot (1 - \frac{\vartheta^2}{2})} \cong \frac{n\Omega}{1 - \beta \sqrt{1 - \frac{\beta_{\perp}^2}{\beta^2}} \cdot (1 - \frac{\vartheta^2}{2})} \cong \\ &\cong \frac{n\Omega}{1 - \beta \cdot (1 - \frac{1}{2} \vartheta^2 - \frac{1}{2} \beta_{\perp}^2)} \cong \frac{2n\Omega \gamma^2}{1 + K^2 + \gamma^2 \vartheta^2} = \frac{\omega_{n \max}}{1 + \frac{\gamma^2 \vartheta^2}{1 + K^2}} \end{aligned} \quad (13)$$

$\beta_{\parallel} = \beta \cdot \sqrt{1 - (\beta_{\perp} / \beta)^2}$  is longitudinal normalized to c velocity,  $\beta_{\perp}$  is transverse normalized velocity,  $K = \beta_{\perp} \gamma$ ,  $\bar{e}$  is unit vector to observer,  $\omega_{n \max} = 2n\gamma^2 \Omega / (1 + K^2)$ .

The amount of energy radiated in solid angle  $d\omega$  on harmonic with number  $n$  can be written as the following, [11]

$$\frac{dI}{d\omega} = \sum_n \frac{dI_n}{d\omega}.$$

<sup>3</sup> We would like to attract attention that in this publication ([12]) there is a mistake in FIG.2 (a). In reality in the rest frame intensity of radiation in x, y direction is not a zero, but is  $1/2$  of maximal, radiated in z direction, factor  $1 + \cos^2 \vartheta$ . In Lab frame the  $\vartheta = 90$  deg angle between y and z goes to  $\sim 1/\gamma$  and the radiation is present under this angle.

In it's turn

$$\frac{dI_n}{do} = \frac{dI_n^+}{do} + \frac{dI_n^-}{do}$$

$$\frac{dI_n^\pm}{do} = I_{tot} \cdot \left[ \frac{3}{4\pi\gamma^4} \frac{n^2 F_n^\pm(K, \gamma)}{(1 - \beta_{\parallel} \cos \vartheta)^3} \right] \equiv I_{tot} \cdot P_n^\pm(K, \vartheta), \quad (14)$$

$$F_n(K, \vartheta) = F_n^+ + F_n^-, \quad F_n^\pm(K, \vartheta) = \frac{1}{2} \left( J_n'(n\kappa) \pm \frac{\cos \vartheta - \beta_{\parallel}}{1 - \beta_{\parallel} \cos \vartheta} \cdot \frac{1}{\kappa} J_n(n\kappa) \right)^2, \quad (15)$$

$$F_n(K, \vartheta) = J_n'^2(n\kappa) + \left( \frac{\cos \vartheta - \beta_{\parallel}}{\beta_{\perp} \sin \vartheta} \right)^2 J_n^2(n\kappa), \quad (16)$$

where  $\kappa = \frac{\beta_{\perp} \sin \vartheta}{1 - \beta_{\parallel} \cos \vartheta}$ .

One can see from (14) that the function in rectangular brackets  $P_n^\pm$  can be treated as density of probability to radiate the photon with certain helicity in polar angle  $\vartheta$ . Really as  $P_n = P_n^+ + P_n^-$

$$\int_o \frac{dI}{do} do = \sum_n \int_o \frac{dI_n}{do} do = I_{tot} \sum_n \int P_n(K, \vartheta) do \equiv I_{tot} \underbrace{\sum_n \int P_n(K, \vartheta) \pi d\vartheta^2}_{=1} = I_{tot}$$

Polarization defined as a ratio

$$\xi_{2n} = \frac{F_n^+ - F_n^-}{F_n} \equiv \frac{F_n^+ - F_n^-}{F_n^+ + F_n^-} = \frac{\partial I_n^+ / \partial \vartheta - \partial I_n^- / \partial \vartheta}{\partial I_n^+ / \partial \vartheta + \partial I_n^- / \partial \vartheta} = 2 \left( \frac{\cos \vartheta - \beta_{\parallel}}{\beta_{\perp} \sin \vartheta} \right) \times \frac{J_n'(n\kappa) J_n(n\kappa)}{F_n(K, \vartheta)} \quad (17)$$

We represented these formulas here for future usage in description of modeling of conversion with numerical code.

In [14] all these formulas were expanded for small argument of Bessel function as (see(8))

$$J_n(x) = \left( \frac{x}{2} \right)^n \sum_{k=0}^{\infty} \frac{(-1)^k}{k! \Gamma(n+k+1)} \equiv \frac{1}{n!} \left( \frac{x}{2} \right)^n - \frac{1}{(n+1)!} \left( \frac{x}{2} \right)^{n+2} + \dots$$

One can also expand

$$\kappa = \frac{\beta_{\perp} \sin \vartheta}{1 - \beta_{\parallel} \cos \vartheta} \equiv \frac{2K\gamma\vartheta}{1 + K^2 + \gamma^2\vartheta^2}, \quad \frac{\cos \vartheta - \beta_{\parallel}}{\beta_{\perp} \sin \vartheta} \equiv \frac{1 + K^2 - \gamma^2\vartheta^2}{2K\gamma\vartheta}$$

For undulator having  $M$  periods in dipole approximation  $K \leq 1$  [14],  $s = \hbar\omega / \hbar\omega_{max}$ ,  $\alpha = e^2 / \hbar c \equiv 1/137.036$

$$\frac{dN_\gamma}{ds} = \sum_n \frac{dN_{\gamma n}}{ds} = 4\pi\alpha M \frac{K^2}{1 + K^2} \sum_n n F_n(K, s) \quad (18)$$

For the first two harmonics

$$\frac{dN_{\gamma n}}{ds} \cong 4\pi\alpha nM \frac{K^2}{1+K^2} \times \begin{cases} \frac{1}{2}(1-2s+2s^2), & n=1 \\ 2s(1-s)(1-s+2s^2), & n=2 \\ \dots \\ F_n(K,s) \end{cases} \quad (19)$$

One can see that the photon spectrum density, normalized to the maximal photon energy for each harmonics  $s = \omega_n / \omega_n^{\max}$  is not a function of energy of primary electron beam

The phonon flux as a function of (not normalized) energy goes respectively

$$\frac{dN_{\gamma n}}{d(\omega_n / \omega_n^{\max})} \rightarrow \frac{dN_{\gamma n}}{d\omega_n} \cong \frac{4\pi\alpha nM}{\omega_n^{\max}} \frac{K^2}{1+K^2} F_n(K,s) = \frac{4\pi\alpha nM}{2\gamma^2\Omega} K^2 F_n(K,s) \quad (20)$$

As the function of the angle the photon density goes to [14]

$$\begin{aligned} \frac{dN_n}{d\vartheta} &= 4\pi\alpha nM \frac{F_n(\vartheta)}{1+K^2+\gamma^2\vartheta^2} \\ F_1(\vartheta) &= \frac{1+\gamma^2\vartheta^2}{2(1+\gamma^2\vartheta^2)^2}, \quad F_2(\vartheta) = 2(K\gamma\vartheta)^2 \frac{1+\gamma^4\vartheta^4}{(1+\gamma^2\vartheta^2)^4}. \end{aligned} \quad (21)$$

Polarization in dipole approximation becomes

$$\xi_{21} = \xi_{22} = \frac{2s-1}{1-2s+2s^2} \quad \text{or} \quad \xi_{21} = \xi_{22} = \frac{1-\gamma^4\vartheta^4}{1+\gamma^4\vartheta^4} \quad (22)$$

One can see, that polarization becomes linear ( $\xi_{21} = \xi_{22} \cong 0$ ), when the angle of observation  $\vartheta \cong 1/\gamma$ .

Total number of the photons radiated at each harmonic from  $s = 1$  (straight forward direction), to the threshold value  $s = s_t$  defined by the maximal possible angle of incoming radiation, selected by the diaphragm

$$\gamma\vartheta_t = \sqrt{(1+K^2)(1-s_t)/s_t}. \quad (23)$$

The number of the photons [14]

$$N_{\gamma n}(K, s_t) = \int_{s_t}^1 \frac{dN_{\gamma n}}{ds} ds = 4\pi\alpha nM \frac{K^2}{1+K^2} \int_{s_t}^1 F_n(K,s) ds \cong 4\pi\alpha nM \frac{K^2}{1+K^2} \Phi_n(K, s_t), \quad (24)$$

In approximation  $\kappa = 2K\sqrt{s(1-s)/(1+K^2)} \leq 1$  ( $K \leq 1$  or/and  $\gamma\vartheta \leq 1$ ) for harmonics with the numbers  $n = 1, 2$

$$N_{n\gamma}(K, s_t) = \int_{s_t}^1 \frac{dN_{\gamma n}}{ds} ds \cong 4\pi\alpha nM \frac{K^2}{1+K^2} \times \begin{cases} \frac{1}{6}(1-s_t)(2-s_t+2s_t^2), & n=1 \\ \frac{K^2}{10 \cdot (1+K^2)} (1-s_t)^2 (1+2s_t-2s_t^2+4s_t^3), & n=2 \\ \dots \end{cases} \quad (25)$$

what is a function of the fractional energy only. The fractional energy  $s_t$  defined by diameter of the diaphragm hole in front of the target

$$s_t \cong \frac{1}{1 + \frac{\gamma^2 d^2}{R^2(1+K^2)}},$$

where  $R$  is the distance to the target from the end of undulator.  $s_t = 0$  corresponds to absence of any selection,  $s_t = 1$  – straight forward direction,  $s_t = 0.8$  selection in 20% down from the maximal possible energy of the quanta. The corresponding maximal values of the angles for selection (minimal value is zero for the forward direction) are

$$\vartheta(s_t = 0.7) = \sqrt{(1+K^2)(1-s_t)/s_t} \cong \frac{0.65\sqrt{1+K^2}}{\gamma} \quad \text{and} \quad \vartheta(s_t = 0.8) \cong \frac{0.5\sqrt{1+K^2}}{\gamma}. \quad (26)$$

If the diaphragm is large,  $\gamma d \geq R$ , then the number of the photons is not a function of the beam energy at all. One can see that for keeping the same fractional energy, it is necessary to keep the ratio  $\gamma d / R$  constant. So reduction of the photon density  $\sim 1/\gamma^2$  is not a limitation.

Polarization of the photons concentrated in the solid angle between 0 and  $\gamma\vartheta_t = \sqrt{(1+K^2)(1-s_t)/s_t}$  (22) can be evaluated as

$$\langle \xi_{2n} \rangle = \frac{\int_{s_t}^1 \xi_{2n}(s) \frac{dN_m}{ds} ds}{\int_{s_t}^1 \frac{dN_m}{ds} ds} = \frac{\int_{s_t}^1 \xi_{2n}(s) \frac{dN_m}{ds} ds}{N_m(K, s_t)}. \quad (27)$$

Using (18), (19) one can obtain

$$\langle \xi_{21} \rangle = \frac{3s_t}{2-s_t+2s_t^2}, \quad \langle \xi_{22} \rangle = \frac{5s_t}{1+2s_t-2s_t^2+4s_t^3}. \quad (28)$$

If system collects only 20% of maximal possible energy down from the maximum, i.e.  $s_t \cong 0.8$ , then

$$\langle \xi_{21} \rangle \cong 0.96, \quad \langle \xi_{22} \rangle \cong 0.95.$$

For  $s_t \cong 0.7$  (30% interval)  $\langle \xi_{21} \rangle \cong 0.92$ ,  $\langle \xi_{22} \rangle \cong 0.89$ . These figures indicate that the level of polarization is high.

According to (26) for  $K=0.1$  the angle under which the target is seen from the end of undulator goes to  $\vartheta(s_t = 0.7) \cong \frac{0.65\sqrt{1+0.01}}{\gamma} \cong 6.5 \cdot 10^{-5}$  rad for  $\gamma = 10^5$ . If we suggest the distance between the undulator and target  $\sim 10$ m, then the increase of the size of gamma spot at the target will be  $\Delta r \cong 10m \times 6.5 \cdot 10^{-5} \cong 0.65$ mm. The increase of the spot due to the angular spread of the SLAC's beam in undulator  $\Delta r_y \cong \sqrt{\epsilon/\beta} \times 10m \cong \sqrt{3 \times 10^{-3} / 300 / 10^5} \times 10m \cong 10^{-5} \times 10m = 0.1$ mm. The last means that angular selection is possible in planned experiment.

For  $K=0.1$  angular and spectral distributions look like the following.

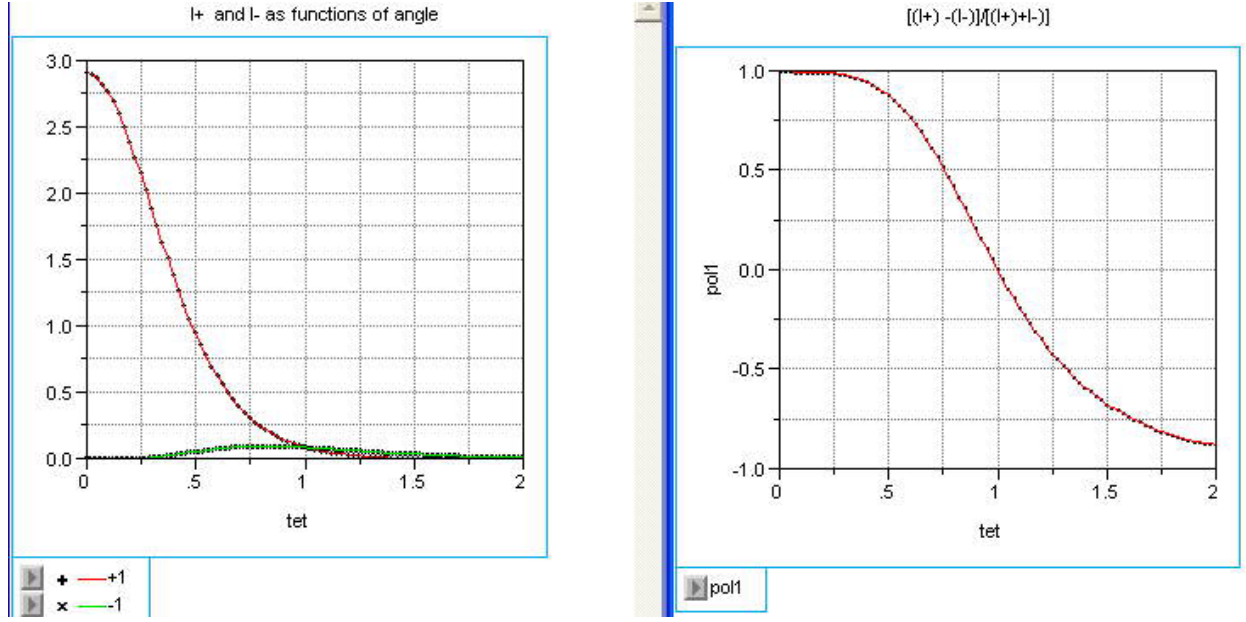


**FIGURE 14:** Angular distribution of intensity for right and left handed helicities as functions of angle  $\partial_{\vartheta} I_1^{\pm}(\vartheta)/I_{tot}$  for the first harmonics, left. Ratio  $\left[ \partial_{\vartheta} I_1^+(\vartheta) - \partial_{\vartheta} I_1^-(\vartheta) \right] / \left[ \partial_{\vartheta} I_1^+(\vartheta) + \partial_{\vartheta} I_1^-(\vartheta) \right]$  formula (17), represented at the right. Undulatority factor  $K=0.1$ ,  $\gamma = 10^5$ , 50 GeV.

Parameter  $s = \omega / \omega_{1max}$  on the graphs is the same as introduced above. Is introduced for each harmonics and can not be more than one, there is no confusion on how to use it for presentation of few harmonics on the same graph, however.

The lowest frequency in the system associated with the photons, radiated backwards,  $\vartheta = \pi$  in formula (13). These photons have the wavelength, which is twice the undulator period  $\lambda_u$ . So strictly speaking there is no radiation below the frequency  $\omega_{th} = \Omega / (1 + \beta_{\parallel}) \cong \pi c / \lambda_u$  what is 4mm radio waves. However restriction occurs even earlier as the vacuum chamber suppresses propagation of the waves with wavelength  $\sim 2a$  (with coefficient  $\sim 1.3065$  for round chamber, so critical wavelength for the chamber with round cross section is  $\lambda_{crit} = 2.613 \cdot a$ ). If however the vacuum chamber is multiply connected, the waves with this lowest frequency can be (coherently for the frequencies  $\pi c / \lambda_u \leq \omega \leq c / \sigma_z^{bunch}$ ) radiated as well.

One can see, that as the frequency of radiation is a function of angle, (13), the spectrum of radiation is a contiguous one if integrated over all angles. The spectrum remains a line type is however the radiation considered under fixed narrow angle.

We would like to say that all formulas represented here valid for infinitely long undulator. For undulator with finite number of periods  $M$  one needs to introduce the factor

$$\left[ \frac{\sin[\pi M n(\omega - \omega_n) / \omega_n]}{n(\omega - \omega_n) / \omega_n} \right]^2$$

into intensity. The length of formation of radiation having wavelength  $\lambda$  is  $l_f \sim 2\gamma^2 \lambda$ . For undulator this is exactly equates to period of undulator. The length of formation of radiation in magnetic field itself is however  $l_B \sim \rho / \gamma = (mc^2 \gamma / eH_{\perp}) / \gamma \cong \lambda_u / K \sim 1.7 \lambda_u$  ( $K=0.1$ ). After this length the photons radiated in angle  $1/\gamma$  from different periods are not interfere.

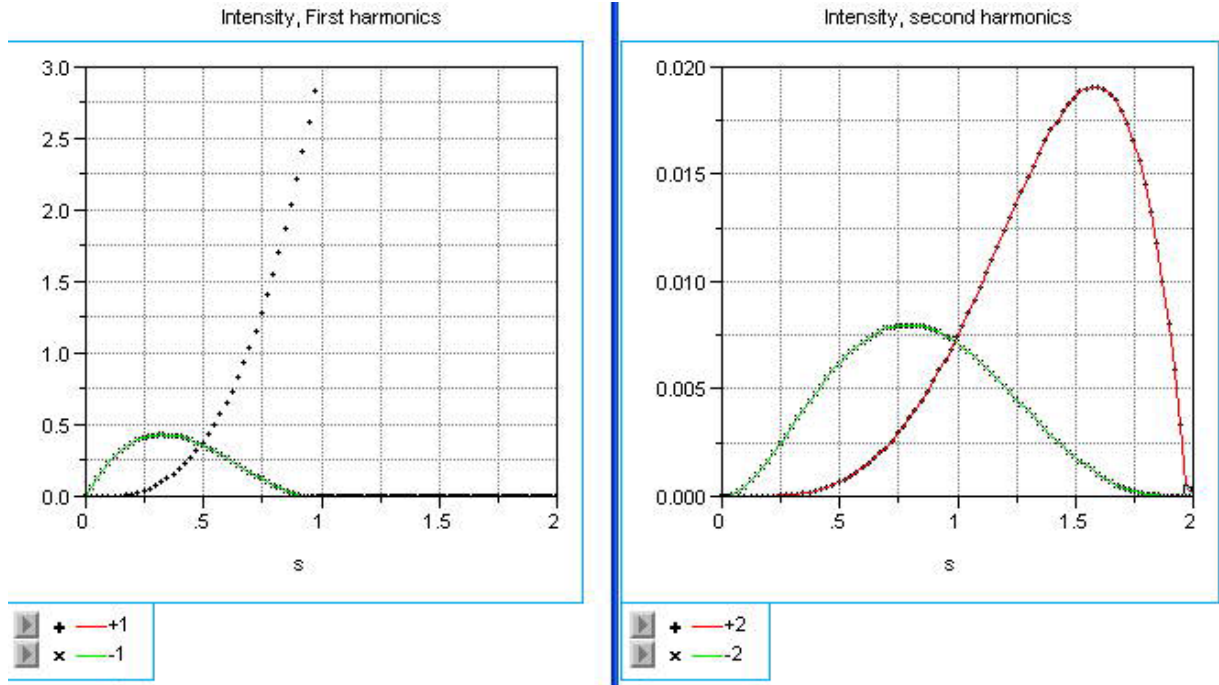


**FIGURE 15:** Spectral distribution of intensity for right and left-handed helicities as functions of normalized frequency  $\frac{\partial I_{1,2}^{\pm}(s)}{I_{tot}} \partial s$  for the first (left) and second (right) harmonics.  $K=0.1$ ,  $\gamma = 10^5$  (50GeV).

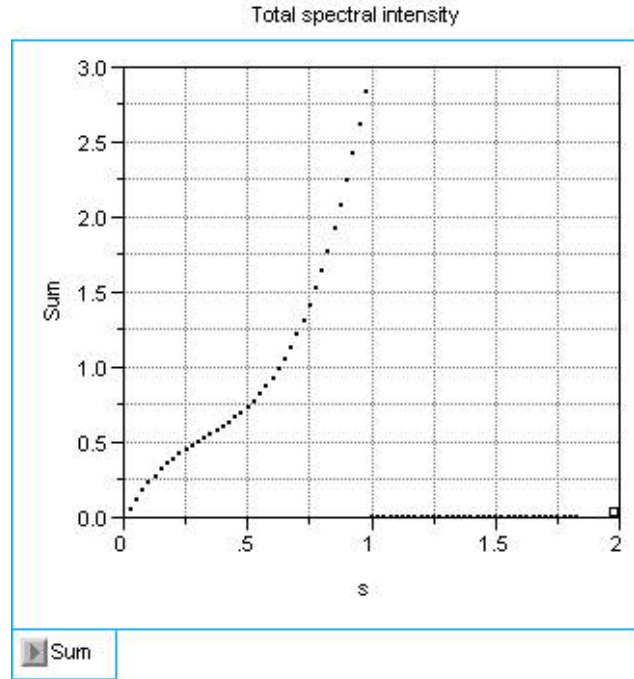


**FIGURE 16:** Total spectral distribution of intensity for right and left-handed helicities as functions of normalized frequency  $\frac{\partial I_1^+(s)}{I_{tot}} \partial s + \frac{\partial I_1^-(s)}{I_{tot}} \partial s + \frac{\partial I_2^+(s)}{I_{tot}} \partial s + \frac{\partial I_2^-(s)}{I_{tot}} \partial s$  for the first and second harmonics.  $K=0.1$ ,  $\gamma = 10^5$ .

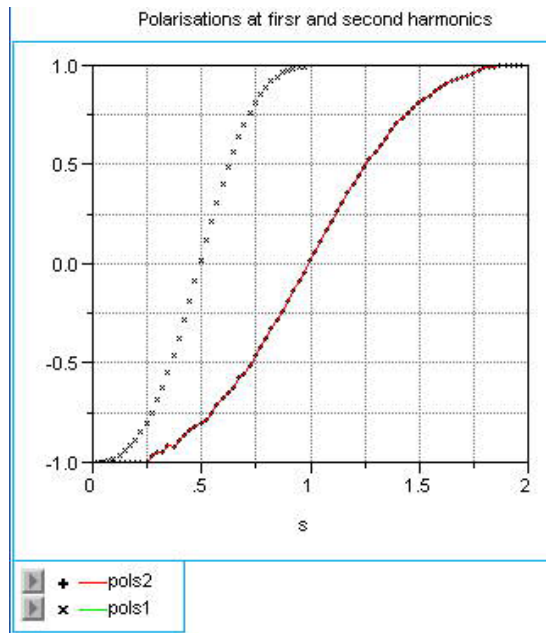


**FIGURE 17:** Spectral distribution of polarization. Basically this is the ratio  $\left[ \frac{\partial I_{1,2}^+(s)}{\partial s} - \frac{\partial I_{1,2}^-(s)}{\partial s} \right] / \left[ \frac{\partial I_{1,2}^+(s)}{\partial s} + \frac{\partial I_{1,2}^-(s)}{\partial s} \right]$  from the graph in Fig.15.

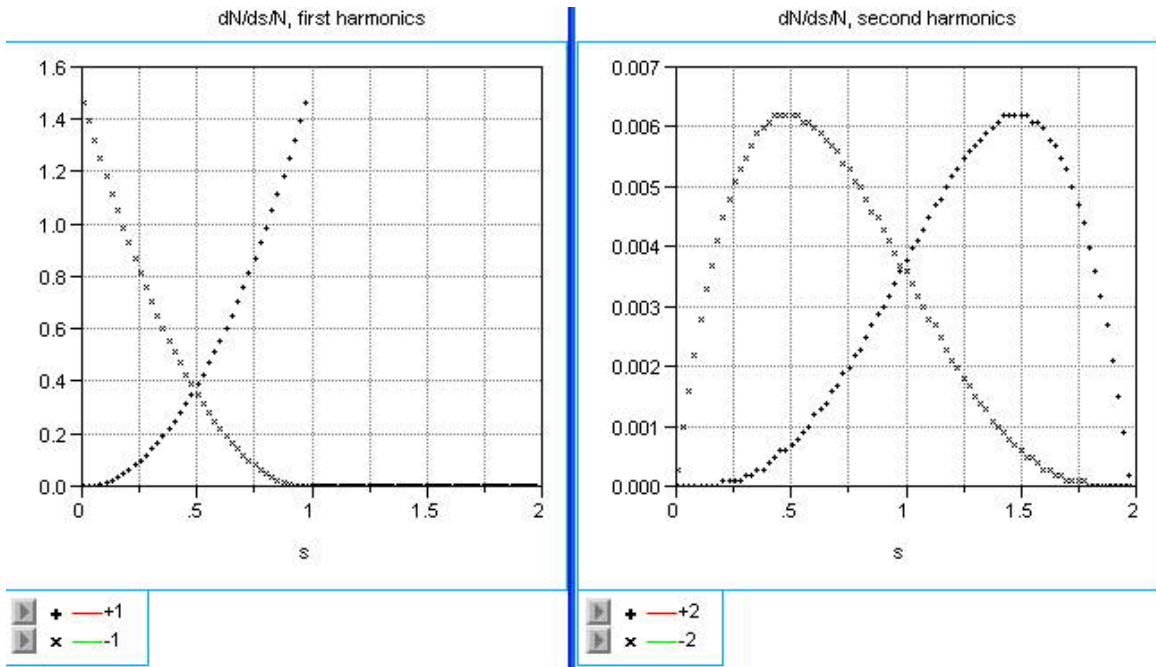


**FIGURE 18:** Spectral distribution of the photon density for the first (left) and second (right) harmonics and for left and right circular polarization for each harmonic. Basically this is  $\frac{\partial N_{1,2}^\pm(s)}{N_{tot} \partial s}$ . Undulatority factor  $K=0.1$ ,  $\gamma = 10^5$ , 50 GeV.

## CONCLUSION

Let us represent here the summary list of parameters.

Parameter	Value
Period	2mm
Axis field	5.6kG
K	~0.1
$\hbar\omega$	12.28MeV(50GeV); 10.4MeV(46GeV)
Losses/particle	$0.1518 \times 10^{-12}$ J/m
Losses	0.948 MeV/m
Number of quants/particle	0.16/m
Feeding current	1.6 kA
Feeding pulse duration	30 $\mu$ s
Heating/pulse	~3 degC
Feeding voltage	1.7V/cm
Average polarization	~90%

One can see, that radiation in the undulator is typical for quantum regime: the amount of energy radiated by particle is less, than energy of quanta. This brings the radiation process in statistical regime.

The questions associated with conversion itself will be considered in other publications.

Summarizing we can say that undulator radiation generated by SLAC's beam has excellent properties for the experiment planned.

Pulsed undulator itself despite its unique parameters looks also a pretty guaranteed from the engineering point of view.

From the table above yields that the undulator having the length  $1/(0.16) \sim 6$  meters will generate one gamma quant per each initial electron(positron).

We believe, however, that for future linear collider an SC undulator with large (~6mm in dia) aperture and ~8mm period is more suitable from the exploitation point of view.

## REFERENCES

- [1] V.Balakin, A. Mikhailichenko, *Conversion system for obtaining highly polarized electrons and positrons at high energy*, Budker INP 79-85, September 13, 1979.
- [2] A.A. Mikhailichenko, *Dissertation*, BINP, Novosibirsk, 1986.
- [3] T.A.Vsevolozskaya, A.A.Mikhailichenko, E.A. Perevedentsev, G.I. Silvestrov, A.D. Cherniakin, *Helical Undulator for Conversion System of the VLEPP Project*, (IYF) BUDKER INP 86-129, Novosibirsk, 1986. XIII International Conference on High Energy accelerators, August 7-11, 1986, Novosibirsk. Proceedings, High-Energy accelerators, vol. 1\* 164-167 and SLAC Stanford - SLAC-TRANS-225, (86, rec.Feb.87) 13 p.
- [4] R.Pitthan, J.Sheppard, *Use of Microundulators to Study Positron Production*, LC02, Proceedings, SLAC-WP-21.

- [5] A.A.Mikhailichenko, *Optimized parameters of the Helical Undulator for test at SLAC*, LC02, Proceedings, SLAC-WP-21.
- [6] A.Mikhailichenko, *SLAC test pulsed undulator concept*, Cornell LEPP CBN 02-7, Aug.16, 2002.
- [7] H. Buchholtz, *Electrische und magnetische Potentiafelder*, Springer-Verlag, 1957.
- [8] V.V.Anshin *et al*, *Superconducting Helical Undulator for the Measurements of Radiation Polarization with Colliding Beams at VEPP-2M*, Budker INP 84-111, 1984.
- [9] Handbook of Mathematical, Scientific and Engineering Formulas, Tables, Functions, Graphs, Transforms, Research and Educational Association, ISBN 0-87891-521-4.
- [10] G.A.Shott, *Electromagnetic radiation and the Mechanical Reactions arising from it*, Cambridge: University Press, 1912.
- [11] D.F. Alferov *et al.*, *The Undulator as a Source of Electromagnetic Radiation*, Particle Acc., vol.9, pp. 223-236(1979).
- [12] B. M. Kincaid, *A Short-period Helical Wiggler as an improved Source of Synchrotron Radiation*, Journal of Applied Phys., Vol. 48, No.7, pp. 2684-2691, July 1977.
- [13] J.P. Blewett, R. Chasman, *Orbits and Fields in helical Wiggler*, Journal of Applied Phys., Vol. 48, No.7, pp. 2692-2698, July 1977.
- [14] E.G. Bessonov, A.A. Mikhailichenko, *Some Aspects of Undulator Radiation formation for the Conversion System of the Linear Collider*, Budker INP 92-43, 1992.